https://doi.org/10.5194/amt-2019-363
Preprint. Discussion started: 14 October 2019

Atmospheric Measurement Techniques Discussions

In situ measurement of CO_2 and CH_4 from aircraft over northeast China and comparison with OCO-2 data

Xiaoyu Sun[1,2], Minzheng Duan[*1,2,3], Yang Gao[4], Rui Han[2,5], Denghui Ji[1,2], Wenxing Zhang[1], Nong Chen[6], Xiangao Xia[1,2], Hailei Liu[3], Yanfeng Huo[7]

[1]LAGEO, Institute of Atmospheric Physics, Chinese Academy of Sciences, 100029 Beijing, China
[2]College of Earth and Planetary Sciences, University of Chinese Academy of Sciences, Beijing,100049, China
[3]Chengdu University of Information Technology, Chengdu, 610225, China,
[4]China Meteorological Administration, Beijing, 100089, China
[5]ICCES, Institute of Atmospheric Physics, Chinese Academy of Sciences, Beijing, 100029, China
[6]Heilongjiang Meteorological Bureau, Harbin, 150001, China
[7]Anhui Meteorology Service, Hefei, 230061, China

Corresponding to: Minzheng Duan (dmz@mail.iap.ac.cn)

Abstract. Several satellites have been launched to monitor the increasing concentrations of greenhouse gases, especially CO_2 and CH_4 in the atmosphere, through back-scattered hyperspectral radiance in the shortwave infrared (SWIR) band. The vertical profiles of greenhouse gases and aerosol could strongly affect the results from these instruments. To investigate the effects of the vertical distribution of CO_2 on uncertainty in SWIR satellite retrieval results, we conducted observations of the vertical profiles of CO_2, CH_4, and aerosol particles at 0.6–7 km above sea level using a Beechcraft King Air 350ER in Jiansanjiang (46.77 °N, 131.99 °E), Heilongjiang province, Northeast China, on August 7–12, 2018. The profiles from this aircraft captured a decrease in CO_2 from 2 km to the minimum altitude due to uptake from vegetation at the surface in summer. CH_4 measurements showed an average 0.5 ppm increase from 2.0 to 0.6 km, which may result from emissions from the large area of paddy fields below, and a constant mole fraction between 1.951 and 1.976 ppm was recorded at 2 km and above. Comparison of CO_2 profiles from a new version of the carbon cycle data assimilation system Tan-Tracker (v1), retrievals from OCO-2 and aircraft measurements was conducted. The results from OCO-2 and the assimilation model system Tan-Tracker captured the vertical structure of CO_2 above 3 km, whereas below 3 km, the values from OCO-2 and Tan-Tracker model were lower than those from in situ measurements. Column-averaged CO_2 volume mixing ratios calculated from in situ measurements showed biases of -2.39 ± 2.02 ppm and -0.61 ± 0.49% compared to OCO-2 retrievals.

1 Introduction

Global warming due to greenhouse gases (GHGs) has become one of the most urgent and widely studied issues facing scientists in recent years. The Fifth Assessment Report of the Intergovernmental Panel on Climate Change (IPCC) noted that the global average temperature has increased by 0.85 °C over the period 1880–2012. GHGs, especially the increasing CO_2 levels in the atmosphere related to anthropogenic activity, are blamed for global warming, because they absorb and emit radiant energy

https://doi.org/10.5194/amt-2019-363
Preprint. Discussion started: 14 October 2019


Atmospheric Measurement Techniques Discussions

within the thermal infrared range. Emission of CO_2 from fossil fuel combustion and industrial processes has contributed about 78% of the total GHG emissions increase from 1970 to 2010 (IPCC, 2015). Accurate measurement of CO_2 concentrations and their spatial and temporal variations in the atmosphere is essential for estimation of sources and sinks in regional and global models. The Global Atmospheric Watch program (http://www.wmo.int/gaw) coordinates the systematic observation and analysis of GHGs and other trace substances, providing an important source of local and global GHG data. However, ground-based and in situ measurements near the surface can only provide information about the lower atmosphere, and are insufficient for analysis of total-column GHGs, which exhibits variations in both vertical and horizontal directions. Over the past few years, several satellites, including the Greenhouse Gases Observing Satellite (GOSAT, launched in January 2009), Second Orbiting Carbon Observatory, (OCO-2, launched in 2014), and TanSat (launched in 2016), have been launched into space to monitor CO_2 by observing back-scattered hyperspectral radiance in shortwave infrared (SWIR) wavelength, which can provide all-weather, all-day global coverage of the column-averaged CO_2 volume mixing ratio (X_{CO2}). Studies have shown that, given a 1–2 ppm accuracy of X_{CO2}, the use of space-borne instrument data can reduce the uncertainties in regional ($8° \times 10°$ footprint) estimation of CO_2 sources and sinks (Rayner and O'Brien, 2001). In addition, CO_2 vertical profiles in the 5–25 km altitude range can be obtained using limb viewing space-borne sounders such as the Atmospheric Chemistry Experiment Fourier Transform Spectrometer (ACE-FTS, launched in August 2003). Foucher et al. (2009) reported the feasibility and difficulties of obtaining vertical CO_2 profiles using this method.

To validate and calibrate the X_{CO2} data from satellite measurement products, the Total Carbon Column Observing Network (TCCON), a network of ground-based solar Fourier transform spectrometers operating in the SWIR spectral region was established (Wunch et al., 2011). Several studies have been conducted to determine X_{CO2}, the column-averaged CH_4 volume mixing ratio (X_{CH4}), and the column-averaged volume mixing ratios of other trace gases (X_{gas}) from TCCON data, which have shown good accuracy (Hedelius et al., 2017; Mendonca et al., 2019). In addition, commercial mobile solar-viewing near-infrared spectrometers of lower resolution than the TCCON instruments, such as Bruker™ EM27/SUN, show potential for measurement of X_{gas} with an acceptable bias range (Hedelius et al., 2016).

Retrieval accuracy is affected by knowledge of the vertical distribution of aerosols and CO_2. Vertical profiles of CO_2 also affect the accuracy of estimation for regional carbon fluxes in transport modeling, and can help elucidate the global carbon cycle and climate change. Many experiments have been conducted to measure the vertical profiles of CO_2, CH_4, and other trace gases. The AirCore sampling system can be used to obtain vertical profiles of CO_2 and CH_4 from near the surface to 8–12 km with high accuracy (Karion et al., 2010; Membrive et al., 2017). Active remote sensing of atmospheric X_{CO2} with the Raman lidar (light detection and ranging) technique has been developed and used to measure CO_2 vertically in the troposphere (Zhao et al., 2007; Gong et al., 2013; Han et al., 2017). CO_2 concentrations were measured at 8–12 km by Tohoku University (Sendai, Japan) through flask sampling on a commercial airliner operated by Japan Airlines (JAL) between Japan and Australia in 1984 and 1985 (Nakazawa et al., 1991). The Comprehensive Observation Network for TRace gases by AIrLiner (CONTRAIL) project installed continuous CO_2 measurement equipment onboard aircraft operated by JAL for in situ measurement (Machida et al., 2008). The data for CONTRAIL are collected at altitudes between a few kilometers and 10 km,

https://doi.org/10.5194/amt-2019-363
Preprint. Discussion started: 14 October 2019


Atmospheric Measurement Techniques Discussions

taking advantage of the frequent movement of commercial aircraft around the world. The Civil Aircraft for Remote Sensing and In Situ Measurements Based on the Instrumentation Container Concept (CARIBIC) project (Brenninkmeijer et al., 1999; Brenninkmeijer et al., 2007) aimed to observe trace gases such as CO, O_3, and CO_2 by deploying measurement equipment in passenger aircraft. The HIAPER Pole-to-Pole Observation (HIPPO) project involved a sequence of five global aircraft measurement programs to sample the atmosphere from near the North Pole to the coastal waters of Antarctica (Wofsy, 2011). Direct measurements that are independently collected from aircraft provide validation information for satellite products. Several studies have shown that profile measurements of CO_2 and CH_4 obtained using aircraft and AirCore are useful for bias correction of both TCCON measurements (Deutscher et al., 2010; Hedelius et al., 2016) and satellite products (Araki et al., 2010; Inoue et al., 2013, 2014; Miyamoto et al., 2013; Frankenberg et al., 2016; Wunch et al., 2017).

Three satellites designed for CO_2 measurement, TanSAT, GMI/GF-5, and GAS/FY-3D, were launched into space in 2016, 2017, and 2018, respectively. Measurement of profiles is crucial to further validate the retrieved hyperspectral measurements from these three satellites. Because the algorithm for satellite retrieval requires a prior profiles based on the model and in situ measurements, the lack of direct and independent airborne observations may increase the bias in the satellite results over China. In this study, in situ aircraft-based measurements of CO_2 and CH_4 were conducted in Jiansanjiang, Northeast China, in August 2018. An ultraportable greenhouse gas analyzer (UGGA; model 915-0011; Los Gatos Research, San Jose, CA, USA) was used onboard the aircraft to measure the vertical mole fractions of CO_2 and CH_4 at altitudes of 0.6–7 km. Descriptions of the aircraft and onboard instruments are provided in Section 2. Details of the experimental site and the flight trajectory are provided in Section 3. A comparison of the profiles obtained using aircraft with OCO-2 and the assimilation system Tan-Tracker (v1) is described in Section 4. Finally, the methods used to calculate X_{CO2} and extrapolate in situ profiles, as well as error estimation, are discussed in Section 5.

2 Instruments

The aircraft used for this experiment was a Beechcraft King Air 350ER, which is a twin-turboprop aircraft designed for weather modification missions and measurement of trace gases and aerosols by the China Meteorological Administration (CMA). The cruising speed and maximum speed of the aircraft are 441 and 561 km/h, respectively. Geolocation data for the aircraft, such as Global Positioning System height, latitude, and longitude, were recorded with the corresponding local time during each flight. Temperature, wind speed, relative humidity, and other meteorological data were detected and recorded by an Aircraft Integrated Meteorological Measurement System (AIMMS) installed on the aircraft.

The ultraportable greenhouse gas analyzer, UGGA (model 915-0011; Los Gatos Research), was connected to an aircraft-based impactor inlet system (CVI Model 1204; Brechtel Manufacturing Inc., Hayward, CA, USA) in the pressurized cabin for continuous measurement of CO_2 and CH_4. The CVI inlet, mounted on top of the aircraft body, maintained an air sample flow rate of 15 L/min using a mass flow controller. The UGGA uses a laser absorption technology called off-axis integrated cavity output spectroscopy to determine the trace gas concentration with a high precision of < 300 ppb (CO_2) and < 2 ppb (CH_4) and

https://doi.org/10.5194/amt-2019-363
Preprint. Discussion started: 14 October 2019


Atmospheric Measurement Techniques Discussions

a 10-s response time. The absolute pressure of the cell was kept constant (66.67 hPa) by an automatic pressure controller, and the absolute temperature was kept within the range of 26.80–33.05 ℃. The UGGA was calibrated against standard GHGs (provided by the National Institute of Metrology, China) before takeoff and after landing of each flight to ensure the accuracy of the data measured with the UGGA. Before this study, the GHG standard gases have been used by the CMA, Chinese Academy of Sciences, and other scientific research institutions for calibration and validation, showing that these standard gases have good performance and reliability.

3 Experimental Site

Aircraft measurement was carried out from August 7 to 10 over Jiansanjiang (47.11 ℃N, 132.66 ℃E, 61 m above sea level), which is located in Heilongjiang province, Northeast China (solid circle, Figure 1). The area is mostly covered with large tracts of farmland. Rice cultivation is carried out primarily in summer, and crop growth is vigorous during this period. Due to the influence of plant photosynthesis, a large amount of CO_2 uptake occurs near the surface. Three profiles were obtained between 08:00 and 11:00 on August 7, 9, and 10.

Figure 2 shows the flight path followed on August 7, when the flight climbed quickly to about 7.5 km after takeoff and then spiraled down toward the surface slowly, over a horizontal distance of about 150 km. Considering the sensitivity of the UGGA response, measurements collected during the ascent were discarded due rapid changes in air pressure, and only data collected and reserved while spiraling downward were regarded as valid and analyzed further. Data recorded below 0.6 km were also rejected because samples were easily contaminated with exhaust emissions during the slowing and descent of the aircraft before landing. The spiral descent of the aircraft lasted for about 2.5 h on each of the three sampling days.

4 Data Processing

4.1 Water vapor correction

The mixing ratio of CO_2 or CH_4 measured during flight is the volume in proportion to air containing water vapor, which cannot be directly compared with values from other data sources due to differing water vapor contents of the sampled air. Therefore, the effect of water vapor is corrected and mixing ratios of CO_2 and CH_4 to dry air are given by:

$$f_{gas\_dry} = \frac{f_{gas} \cdot p}{p - p_{H_2O}} \quad (1)$$

where f_{gas_dry} (mol/mol) is the mole fraction of a gas in dry air, and f_{gas} (mol/mol) is the measured mole fraction of gas under real air conditions with water vapor. P_{H_2O} is water vapor pressure in hPa, which can be calculated as:

$$p_{H_2O} = e_s \cdot RH \quad (2)$$

https://doi.org/10.5194/amt-2019-363
Preprint. Discussion started: 14 October 2019


Atmospheric Measurement Techniques Discussions

where e_s (hPa) is the saturated water vapor pressure at temperature T (K) at aircraft altitudes, which can be derived from the Clausius–Clapeyron equation:

$$\ln\frac{e_s}{6.11}=\frac{L_v M_w}{R}\left(\frac{1}{273}-\frac{1}{T}\right)\approx 5.42\times10^3\left(\frac{1}{273}-\frac{1}{T}\right). \quad (3)$$

where L_v is the latent heat of vaporization, M_w is the molecular weight of water, and R is the gas constant. Temperature T (K), relative humidity RH (%), and pressure p (hPa) of the ambient atmosphere are measured using the aircraft meteorology system, AIMMS.

4.2 Data interpolation

Before aircraft takeoff, the clocks of both the UGGA and AIMMS were adjusted to match those of the CO_2, CH_4, and weather system measurements, synchronizing these data to the altitude and geolocation of the aircraft. The data from UGGA and synchronous meteorology measurements, including temperature, pressure, and humidity of ambient atmosphere, are recorded every second, then smoothed with a 10-s running average to further remove errors caused by temporal mismatch considering the response time of the UGGA. Because the flights followed a spiral trajectory that descended approximately every 300 m, only data collected during level flight were retained and analyzed, whereas data from the descent periods were removed to avoid effects from vertical variations in sampling during rapid descent.

5 Results and Discussion

5.1 CO_2 and CH_4 profiles

Figure 3 shows vertical profiles of the CO_2 and CH_4 mole fractions measured with the UGGA during the flight campaign over Jiansanjiang, which is an agricultural area that produces a large amount of rice. The CO_2 concentration increased with height in the troposphere (Figure 3a), which may have resulted from CO_2 uptake by rice plants near the surface during the summer growth season. The greater increase rate of CO_2 in the lower troposphere on August 7 compared to the other two days was attributed to differing weather conditions on the three sampling days. August 7 was a sunny day, but it was overcast on August 9 and 10, which may have weakened photosynthesis in rice and reduced CO_2 uptake. During all three flights, the mole fraction of CO_2 reached a maximum of about 418 ppm in the free troposphere at the top of the profile.

The mixing ratio of CH_4 showed a consistent decrease in concentration with height, ranging from 1.95 to 2.10 ppm from about 2 km to near the surface, which may have been the result of CH_4 emissions from agricultural activity at the surface. CH_4 showed low variability of less than 0.5 ppm at higher altitudes, from above 2 to 7 km, indicating a well-mixed vertical structure of CH_4 in the free troposphere.

Comparing the CO_2 and CH_4 observation data, the mole fraction of CH_4 varied less than that of CO_2 from 1.5–2 km up to the free troposphere, with a stable value of about 1.925 ppm. This stability indicated that CH_4 was evenly mixed at these heights and that there were no obvious sources or sinks of CH_4. Conversely, CO_2 rose with increasing altitude in the free troposphere

https://doi.org/10.5194/amt-2019-363
Preprint. Discussion started: 14 October 2019


Atmospheric Measurement Techniques Discussions

from about 400 to 418 ppm. This increase may have been due to photosynthesis by vegetation and the large number of crops planted locally, creating a CO_2 sink at the surface, and causing the CO_2 concentration to rise with height in the free troposphere. Our findings indicate that the vertical profile of CO_2 in summer increases with height in the upper troposphere, whereas that of CH_4 changes little with height and is relatively stable.

5.2 Comparison of profiles from the model and satellite product

Aircraft measurements were compared with CO_2 data obtained from OCO-2 (v9r) retrievals and the recently developed data assimilation system for the global carbon cycle, Tan-Tracker (v1) (Han and Tian, 2019). Based on the nonlinear least squares four-dimensional variational data assimilation algorithm (NLS-4DVar) and the Goddard Earth Observing System atmospheric chemistry transport model (GEOS-Chem), Tan-Tracker provides accurate surface flux inversion estimates and profiles of CO_2 with 47 levels of vertical resolution from the surface to 0.03 hPa and horizontal resolution of $2.5° \times 2°$. The assimilation data are collected and linearly interpolated spatially and temporally based on the geolocation of the observation site and time.

The variation of CO_2 with height could be roughly divided into three segments: surface to 2 km, 2 to 3 km, and 3 to 8 km (Figure 4). Below 2 km, CO_2 is assumed to be well mixed and uniformly distributed with height, with values ranging from 385 to 395 ppm; therefore, the model could not reproduce the strong decrease in CO_2 from 2 km to the surface due to uptake by vegetation. From 2 to 3 km, CO_2 increased to about 400 ppm with altitude. The averaged satellite retrieval profiles correctly reproduced the decrease in CO_2 from 2 km to the surface, but the decrease rate was lower than those of in situ profiles, decreasing from 393 ppm at 2 km to 390 ppm near the surface. Flight data showed a significant CO_2 sink in this region, most notably on August 7, when it decreased from 400 ppm at 2 km to 380 ppm at 0.6 km. The impact of ground sinks was more pronounced and apparent than in results from satellite inversion and model simulations, indicating that the strong variations in the lower atmosphere and planetary boundary layer (PBL) should be more carefully considered in modeling and retrieval algorithms. Between 2 and 4 km, aircraft profiles showed a relatively uniform mixing level of CO_2, with roughly stable concentrations around 400 ppm.

In general, all profiles from aircraft, satellite retrieval, and modeling showed a similar vertical distribution trend in the troposphere above 2 km, but with large differences in values. The volume mixing ratios of CO_2 from both satellite and aircraft measurements indicated a CO_2 sink.

5.3 Comparison of X_{CO2} products

The total column amount of CO_2, can be derived by integrating the CO_2 concentration from the surface to the top of the atmosphere under the assumption of hydrostatic conditions:

$$VC_{CO_2} = \int_0^{P_s} \frac{f_{CO_2}^{dry} \cdot (1 - f_{H_2O})}{g(p) \cdot m(p)} dp \qquad (4)$$

$$m = [m_{H_2O} \cdot f_{H_2O} + m_{air}^{dry} \cdot (1 - f_{H_2O})]$$

https://doi.org/10.5194/amt-2019-363
Preprint. Discussion started: 14 October 2019

Atmospheric Measurement Techniques Discussions

where VC_{CO_2} is the total column amount of CO_2, $f_{CO_2}^{dry}$ is the dry-air mole fraction (DMF) of CO_2 (mol mol^{-1}), $f_{H_2O}(p)$ is the aircraft profile of H_2O (mol mol^{-1}), which is measured using the onboard AIMMS system, m(p) is the mean molecular mass of wet air, and g(p) is gravitational acceleration, $m_{H_2O} = 18.02 \times 10^{-3}/N_A$ kg/molecule, $m_{air}^{dry} = 28.964 \times 10^{-3}/N_A$ kg/molecule, and N_A is Avogadro's constant. Data beyond the flight limit are taken from National Centers for Environmental Prediction (NCEP) reanalysis data interpolated to the time of flight.

The column-averaged DMF of CO_2 (X_{CO2}) from aircraft measurements was calculated based on the method of Wunch et al. (2010), which considers the average kernel in OCO-2 satellite retrievals:

$$X_{CO_2}^{\text{in situ}} = X_{CO_2}^{a} + \sum_j h_j a_j (t_{\text{in situ}} - t_a)_j \quad (5)$$

where a is the average kernel (Rodgers and Connor, 2003), $X_{CO_2}^{a}$ is the column-averaged DMF for the a priori profile t_a, h_j is the pressure weighting function of OCO-2, and $t_{\text{in situ}}$ is the in situ profile from aircraft measurement.

Because in situ measurements available from aircraft are limited, values outside of the aircraft's vertical observation range must be estimated to calculate X_{CO2}. A well-mixed and constant mixing ratio of CO_2 is assumed from the surface to the lower limit of flight, and from the upper limit of flight to the tropopause. The CO_2 concentrations for the stratosphere and above were calculated with an empirical model (Toon and Wunch, 2014) that considers tropopause height as well as realistic latitude and time dependencies through curve fitting of data from methods such as high-altitude balloons, AirCore, Observations of the Middle Stratosphere balloon, and aircraft. In general, the mole fraction of CO_2 decreased exponentially with height from the tropopause to upper stratosphere, and the tropopause height was obtained from NCEP reanalysis data with a $2.5° \times 2.5°$ resolution, which was linearly interpolated to the geographic coordinates of Jiansanjiang. X_{CO2} calculated from aircraft measurements and differences with that from OCO-2 are listed in Table 1. Because no data were obtained from OCO-2 over Jiansanjiang during the flight, the results of OCO-2 within $1° \times 1°$ spatially at the closest time to the flight, which were collected on August 5, were used for comparison. The results showed that X_{CO2} values from OCO-2 were lower, with an average difference of -2.39 ± 2.02 ppm ($-0.59\% \pm 0.44\%$).

Uncertainties induced by extrapolation of profiles outside the height limits of aircraft flight and by errors in tropopause estimation were analyzed. Errors in extrapolation of the profile below the lower limit and above the upper limit of flight were estimated by recalculating X_{CO2} after a 1-ppm positive shift in the CO_2 concentrations at these altitudes. As the profile is assumed to decrease exponentially with height above the tropopause, the height of the tropopause also introduces uncertainties for X_{CO2}. Table 2 lists the errors resulting from three sources: 1) uncertainties from in situ measurement, 2) extrapolation of the profile in the PBL where no in situ measurements were collected, and 3) profile assumptions above the upper limit of flight observations. Errors due to uncertainty in tropopause height were analyzed by shifting the tropopause height upward by 1 km, and the results are also listed in Table 2. These results indicated that the extrapolation method and assumptions used to construct profiles where no measurements were made were the primary source of errors, among which the greatest error was from the

https://doi.org/10.5194/amt-2019-363
Preprint. Discussion started: 14 October 2019


Atmospheric Measurement Techniques Discussions

profile above the upper limit of the flight (0.34 ppm, 0.85%). Errors due to uncertainty in the tropopause height were also non-negligible.

6 Conclusion

The vertical distributions of CO_2 and CH_4 were measured using a Beechcraft King Air 350ER over Jiansanjiang, an extensive paddy area in Northeast China, and three vertical profiles from 0.6 to 7.5 km were obtained on August 7, 9, and 10. Measurements of the mole fraction of CO_2 showed an increase with height, whereas CH_4 decreased with height. These results are reasonable, because paddies are a sink for CO_2 and source of CH_4 during the summer growing season. Comparing the observed profiles from aircraft with those from the carbon cycle data assimilation system Tan-Tracker (v1) and OCO-2 retrievals showed that the general vertical structure was consistent, but the values of mole fraction of CO_2 from Tan-Tracker and OCO-2 had negative bias estimates of -2.39 ± 2.02 ppm and 0.59 ± 0.44%, respectively. The uncertainty arose mainly from extrapolation of the profile beyond the flight limit, where no in situ measurements were available.

Data availability

Data used in this study are available from the corresponding author upon request (dmz@mail.iap.ac.cn).

Author contributions

M. Duan and X. Sun determined the main goal of this study. X. Sun carried it out, analyzed the data, and prepared the paper with contributions from all co-authors. Y. Gao and N. Chen provided technical guidance for related instrument.

Competing interests

The authors declare that they have no conflict of interest.

Acknowledgements

This work is supported by the National Nature Science Foundation of China (No. 41527806 and No.41705014). We also acknowledge numerous staff of the Weather Modification Center, China Meteorological Administration, for supporting the experiment and the instrumentation onboard the aircraft. We also thank Jiansanjiang Airport for providing the experimental site and arranging time for conducting the campaign.

https://doi.org/10.5194/amt-2019-363
Preprint. Discussion started: 14 October 2019

Atmospheric Measurement Techniques Discussions

References

Araki, M., Morino, I., Machida, T., Sawa, Y., Matsueda, H., Ohyama, H., Yokota, T., and Uchino, O.: CO_2 column-averaged volume mixing ratio derived over Tsukuba from measurements by commercial airlines, Atmos. Chem. Phys., 10, 7659–7667, https://doi.org/10.5194/acp-10-7659-2010, 2010.

Brenninkmeijer, C., Crutzen, P., Boumard, F., Dauer, T., Dix, B., Ebinghaus, R., Filippi, D., Fischer, H., Franke, H., and Frieβ, U.: Civil Aircraft for the regular investigation of the atmosphere based on an instrumented container: The new CARIBIC system, Atmos. Chem. Phys., 7, 4953–4976, https://doi.org/10.5194/acp-7-4953-2007, 2007.

Brenninkmeijer, C., Crutzen, P., Fischer, H., Güsten, H., Hans, W., Heinrich, G., Heintzenberg, J., Hermann, M., Immelmann, T., and Kersting, D.: CARIBIC—Civil aircraft for global measurement of trace gases and aerosols in the tropopause region, J. Atmos. Ocean, Tech., 16, 1373–1383, https://doi.org/10.1175/1520-0426(1999)016<1373:CCAFGM>2.0.CO;2, 1999.

Deutscher, N., Griffith, D., Bryant, G., Wennberg, P., Toon, G., Washenfelder, R., Keppel-Aleks, G., Wunch, D., Yavin, Y., and Allen, N.: Total column CO_2 measurements at Darwin, Australia-site description and calibration against in situ aircraft profiles, Atmos. Meas. Tech., 3, 947–958, https://doi.org/10.5194/amt-3-947-2010, 2010.

Foucher, P., Chédin, A., Dufour, G., Capelle, V., Boone, C., and Bernath, P.: Feasibility of CO_2 profile retrieval from limb viewing solar occultation made by the ACE-FTS instrument, Atmos. Chem. Phys., 9, 2873–2890, https://doi.org/10.5194/acp-9-2873-2009, 2009.

Frankenberg, C., Kulawik, S. S., Wofsy, S. C., Chevallier, F., Daube, B., Kort, E. A., O'dell, C., Olsen, E. T., and Osterman, G.: Using airborne HIAPER Pole-to-Pole Observations (HIPPO) to evaluate model and remote sensing estimates of atmospheric carbon dioxide, Atmos. Chem. Phys., 16, 7867–7878, https://doi.org/10.5194/acp-16-7867-2016, 2016.

Gong, W., Han, G., Ma, X., and Lin, H.: Multi-points scanning method for wavelength locking in CO_2 differential absorption lidar, Opt. Commun., 305, 180–184, https://doi.org/10.1016/j.optcom.2013.05.006, 2013.

Han, G., Ma, X., Liang, A., Zhang, T., Zhao, Y., Zhang, M., and Gong, W.: Performance evaluation for China's planned CO_2-IPDA, Remote Sens., 9, 768, https://doi.org/10.3390/rs9080768, 2017.

Han, R. and Tian, X.: A dual-pass carbon cycle data assimilation system to estimate surface CO2 fluxes and 3D atmospheric CO2 concentrations from spaceborne measurements of atmospheric CO2, Geosci. Model Dev. Discuss., https://doi.org/10.5194/gmd-2019-54, in review, 2019.

Hedelius, J. K., Parker, H., Wunch, D., Roehl, C. M., Viatte, C., Newman, S., Toon, G. C., Podolske, J. R., Hillyard, P. W., Iraci, L. T., Dubey, M. K., and Wennberg, P. O.: Intercomparability of X_{CO2} and X_{CH4} from the United States TCCON sites, Atmos. Meas. Tech., 10, 1481–1493, https://doi.org/10.5194/amt-10-1481-2017, 2017.

Hedelius, J. K., Viatte, C., Wunch, D., Roehl, C. M., Toon, G. C., Chen, J., Jones, T., Wofsy, S. C., Franklin, J. E., Parker, H., Dubey, M. K., and Wennberg, P. O.: Assessment of errors and biases in retrievals of X_{CO2}, X_{CH4}, X_{CO}, and X_{N2O} from a 0.5 cm–1 resolution solar-viewing spectrometer, Atmos. Meas. Tech., 9, 3527–3546, https://doi.org/10.5194/amt-9-3527-2016, 2016.

https://doi.org/10.5194/amt-2019-363
Preprint. Discussion started: 14 October 2019

Inoue, M., Morino, I., Uchino, O., Miyamoto, Y., Saeki, T., Yoshida, Y., Yokota, T., Sweeney, C., Tans, P., Biraud, S., Machida, T., Pittman, J. V., Kort, E. A., Tanaka, T., Kawakami, S., Sawa, Y., Tsuboi, K., and Matsueda, H.: Validation of XCH 4 derived from SWIR spectra of GOSAT TANSO-FTS with aircraft measurement data, Atmos. Meas. Tech., 7, 2987–3005, https://doi.org/10.5194/amt-7-2987-2014, 2014.

Inoue, M., Morino, I., Uchino, O., Miyamoto, Y., Yoshida, Y., Yokota, T., Machida, T., Sawa, Y., Matsueda, H., Sweeney, C., Tans, P. P., Andrews, A. E., Biraud, S. C., Tanaka, T., Kawakami, S., and Patra, P. K.: Validation of X_{CO2} derived from SWIR spectra of GOSAT TANSO-FTS with aircraft measurement data, Atmos. Chem. Phys., 13, 9771–9788, https://doi.org/10.5194/acp-13-9771-2013, 2013.

Karion, A., Sweeney, C., Tans, P., and Newberger, T.: AirCore: An innovative atmospheric sampling system, J. Atmos. Ocean, Tech., 27, 1839–1853, https://doi.org/10.1175/2010JTECHA1448.1, 2010.

Machida, T., Matsueda, H., Sawa, Y., Nakagawa, Y., Hirotani, K., Kondo, N., Goto, K., Nakazawa, T., Ishikawa, K., and Ogawa, T.: Worldwide measurements of atmospheric CO_2 and other trace gas species using commercial airlines, J. Atmos. Ocean, Tech., 25, 1744–1754, https://doi.org/10.1175/2008JTECHA1082.1, 2008.

Membrive, O., Crevoisier, C., Sweeney, C., Danis, F., Hertzog, A., Engel, A., Bönisch, H., and Picon, L.: AirCore-HR: a high-resolution column sampling to enhance the vertical description of CH_4 and CO_2, Atmos. Meas. Tech., 10, 2163-2181, https://doi.org/https://doi.org/10.5194/amt-10-2163-2017, 2017.

Mendonca, J., Strong, K., Wunch, D., Toon, G. C., Long, D. A., Hodges, J. T., Sironneau, V. T., and Franklin, J. E.: Using a speed-dependent Voigt line shape to retrieve O_2 from Total Carbon Column Observing Network solar spectra to improve measurements of X_{CO2}, Atmos. Meas. Tech., 12, 35–50, https://doi.org/10.5194/amt-12-35-2019, 2019.

Miyamoto, Y., Inoue, M., Morino, I., Uchino, O., Yokota, T., Machida, T., Sawa, Y., Matsueda, H., Sweeney, C., Tans, P. P., Andrews, A. E., and Patra, P. K.: Atmospheric column-averaged mole fractions of carbon dioxide at 53 aircraft measurement sites, Atmos. Chem. Phys., 13, 5265–5275, https://doi.org/10.5194/acp-13-5265-2013, 2013.

Miyamoto, Y., Inoue, M., Morino, I., Uchino, O., Yokota, T., Machida, T., Sawa, Y., Matsueda, H., Sweeney, C., Tans, P. P., Andrews, A. E., Biraud, S. C., and Patra, P. K.: Corrigendum to "Atmospheric column-averaged mole fractions of carbon dioxide at 53 aircraft measurement sites" published in Atmos. Chem. Phys. 13, 5265–5275, 2013, Atmos. Chem. Phys., 13, 9213–9216, https://doi.org/10.5194/acp-13-9213-2013, 2013.

Nakazawa, T., Miyashita, K., Aoki, S., and Tanaka, M.: Temporal and spatial variations of upper tropospheric and lower stratospheric carbon dioxide, Tellus., 43, 106–117, https://doi.org/10.1034/j.1600-0889.1991.t01-1-00005.x, 2010.

O'Brien, D. and Rayner, P.: Global observations of the carbon budget, 2, CO_2 column from differential absorption of reflected sunlight in the 1.61 μm band of CO_2, J. Geophys. Res.-Atmos., 107, ACH 6-1-ACH 6–16, https://doi.org/10.1029/2001JD000617, 2002.

Pachauri, R. K., Allen, M. R., Barros, V. R., Broome, J., Cramer, W., Christ, R., Church, J. A., Clarke, L., Dahe, Q., and Dasgupta, P.: Climate change 2014: synthesis report. Contribution of Working Groups I, II and III to the fifth assessment report of the Intergovernmental Panel on Climate Change, 151, 2014.

https://doi.org/10.5194/amt-2019-363
Preprint. Discussion started: 14 October 2019

Pei-Tao, Z., Yin-Chao, Z., Lian, W., Yue-Feng, Z., Jia, S., Xin, F., Kai-Fa, C., Jun, X., and Xiao-Yong, D.: Analysis of influence of atmosphere extinction to Raman lidar monitoring CO_2 concentration profile, Chin. Phys., 16, 2486, https://doi.org/10.1088/1009-1963/16/8/055, 2007.

Rayner, P. and O'Brien, D.: The utility of remotely sensed CO_2 concentration data in surface source inversions, Geophys. Res. Lett., 28, 175–178, https://doi.org/10.1029/2000GL011912, 2001.

Rodgers, C. D. and Connor, B. J.: Intercomparison of remote sounding instruments, J. Geophys. Res.-Atmos., 108, 4116, https://doi.org/10.1029/2002JD002299, 2003.

Toon, G. C. and Wunch, D.: A stand-alone a priori profile generation tool for GGG2014, TCCON data archive, hosted by the Carbon Dioxide Information Analysis Center, Oak Ridge National Laboratory, Oak Ridge, Tennessee, U.S.A., https://doi: 10.14291/tccon.ggg2014.priors.R0/1221661, 2014.

Wofsy, S. C.: HIAPER Pole-to-Pole Observations (HIPPO): fine-grained, global-scale measurements of climatically important atmospheric gases and aerosols, Philos. Trans. Royal Soc. A, 369, 2073–2086, https://doi.org/doi.org/10.1098/rsta.2010.0313, 2011.

Wunch, D., Toon, G. C., Blavier, J.-F. L., Washenfelder, R. A., Notholt, J., Connor, B. J., Griffith, D. W., Sherlock, V., and Wennberg, P. O.: The total carbon column observing network, Philos. Trans. Royal Soc. A, 369, 2087–2112, https://doi.org/10.1098/rsta.2010.0240, 2011.

Wunch, D., Toon, G. C., Wennberg, P. O., Wofsy, S. C., Stephens, R. S., Fischer, M. K., Uchino, O., Abshire, J., Bernath, P., Biraud, S. C., Blavier, J.-F. L., Boone, C., Bowman, K. P., Browell, E. V., Campos, T., Connor, B. J., Daube, B. C., Deutscher, N. M., Diao, M., Elkins, J. W., Gerbig, C., Gottlieb, E., Griffith, D. W. T., Hurst, D. F., Jiménez, R., Keppel-Aleks, G., Kort, E. A., Macatangay, R., Machida, T., Matsueda, H., Moore, F., Morino, I., Park, S., Robinson, J., Roehl, C. M., Sawa, Y., Sherlock, V., Sweeney, C., Tanaka, T., and Zondlo, M. A.: Calibration of the Total Carbon Column Observing Network using aircraft profile data, Atmos. Meas. Tech., 3, 1351–1362, https://doi.org/10.5194/amt-3-1351-2010, 2010.

Wunch, D., Wennberg, P. O., Osterman, G., Fisher, B., Naylor, B., Roehl, C. M., O'Dell, C., Mandrake, L., Viatte, C., Kiel, M., Griffith, D. W. T., Deutscher, N. M., Velazco, V. A., Notholt, J., Warneke, T., Petri, C., Maziere, M. D., Sha, M. K., Sussmann, R., Rettinger, M., Pollard, D., Robinson, J., Morino, I., Uchino, O., Hase, F., Blumenstock, T., Feist, D. G., Arnold, S. G., Strong, K., Mendonca, J., Kivi, R., Heikkinen, P., Iraci, L., Podolske, J., Hillyard, P. W., Kawakami, S., Dubey, M. K., Parker, H. A., Sepulveda, E., García, O. E., Te, Y., Jeseck, P., Gunson, M. R., Crisp, D., and Eldering, A.: Comparisons of the Orbiting Carbon Observatory-2 (OCO-2) X_{CO2} measurements with TCCON, Atmos. Meas. Tech., 10, 2209–2238, https://doi.org/10.5194/amt-10-2209-2017, 2017.

https://doi.org/10.5194/amt-2019-363
Preprint. Discussion started: 14 October 2019

Atmospheric Measurement Techniques Discussions

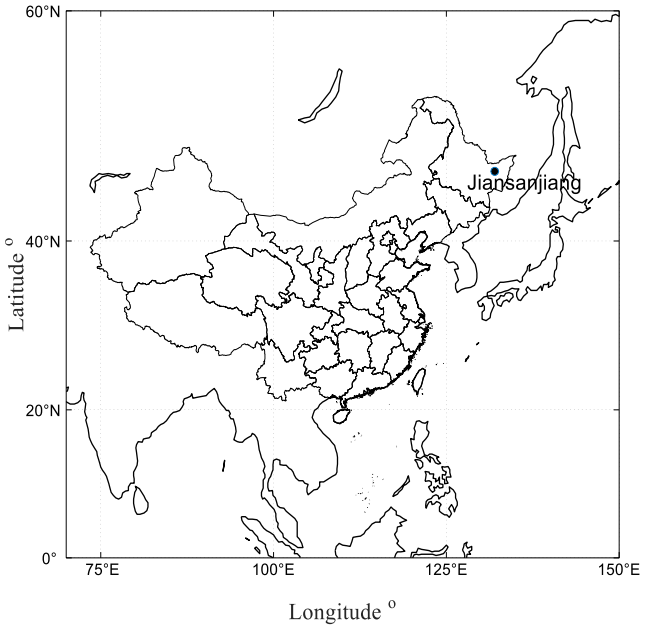

330 **Figure 1. Observation area for aircraft-based measurement of CO2 and CH4 over Jiansanjiang, Northeast China.**

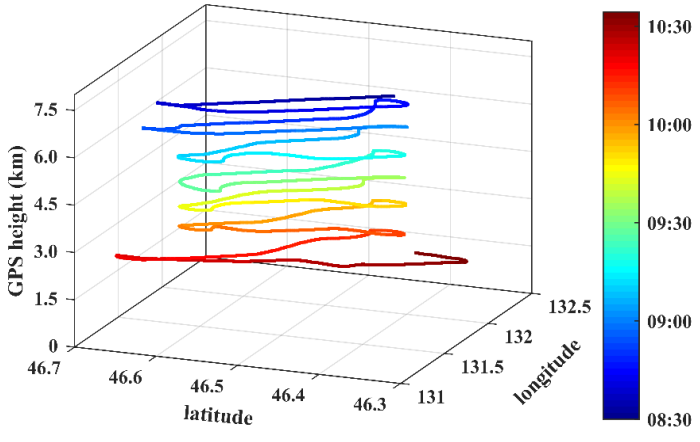

Figure 2. Trajectory of the August 7 flight in Jiansanjiang. The color scale shows the progression of time in local time, where blue represents the start time of the data profile, and red represents the end time.

https://doi.org/10.5194/amt-2019-363
Preprint. Discussion started: 14 October 2019

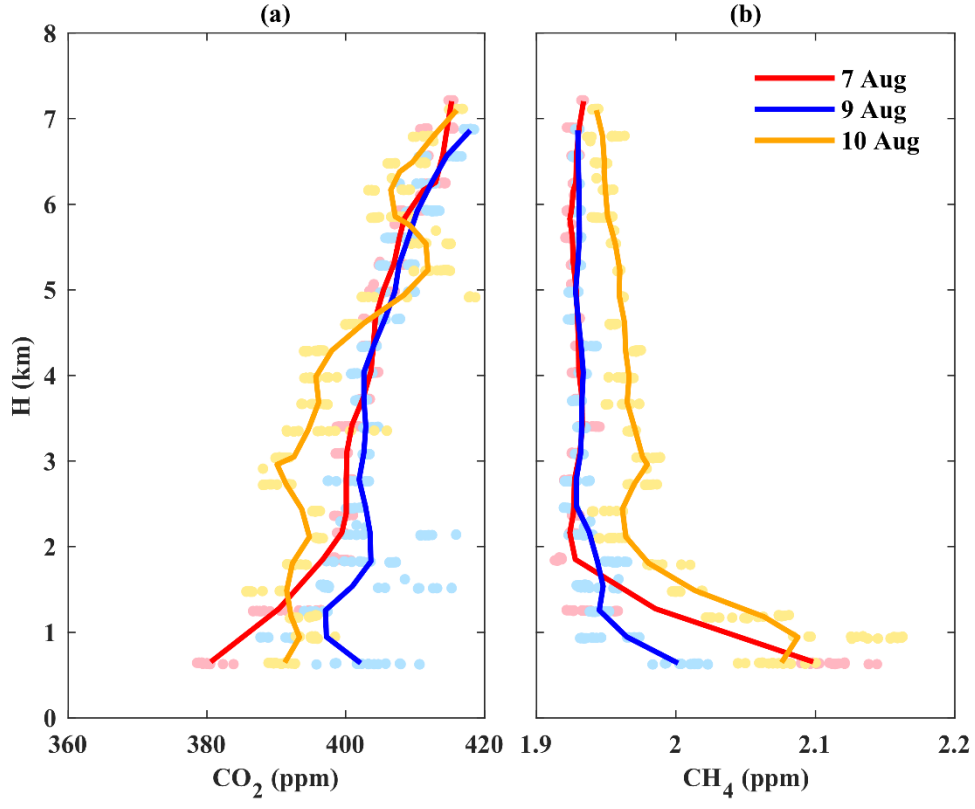

335 **Figure 3. Vertical profiles of (a) CO2 and (b) CH4 observed on August 7 (blue), 9 (red), and 10 (yellow), 2018, over Jiansanjiang measured in situ with aircraft. The aircraft-based in situ measurement data are indicated with dots, and averaged data for each flat flight stage are shown as lines.**

https://doi.org/10.5194/amt-2019-363
Preprint. Discussion started: 14 October 2019

Atmospheric Measurement Techniques Discussions

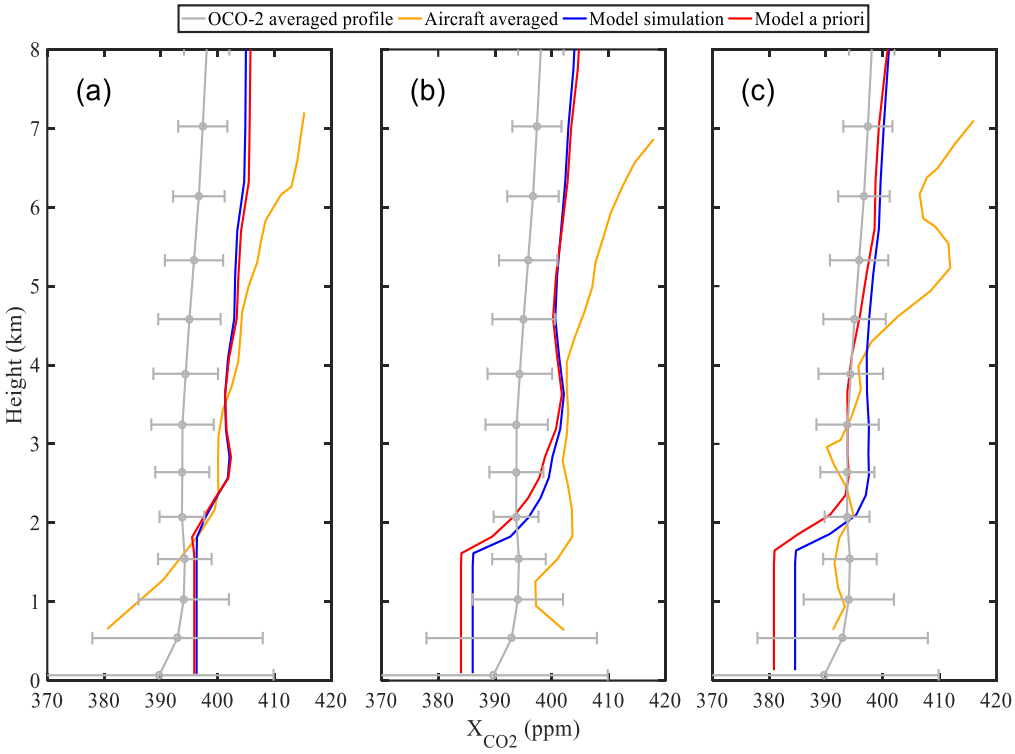

Figure 4. Comparison of aircraft measurements (in situ measurement data are shown as circles, and averaged data for each flat flight stage is indicated by the red line) collected on August (a) 7, (b) 9, and (c) 10, Tan-Tracker (v1) data (blue line) at the location of Jiansanjiang linearly interpolated to the observation times on August (a) 7, (b) 9, and (c) 10, and the OCO-2 averaged profile (gray line) for the aircraft flight area from August 5 with 1 standard deviation (gray bars).

https://doi.org/10.5194/amt-2019-363
Preprint. Discussion started: 14 October 2019

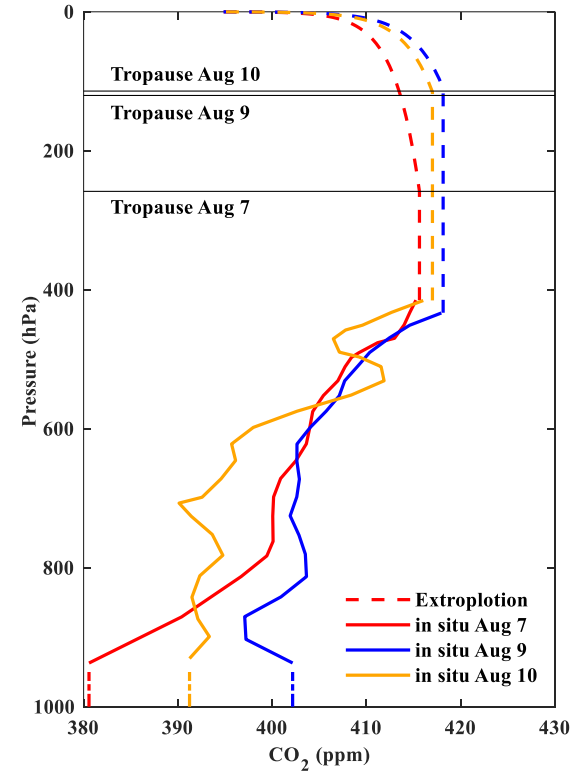

Figure 5. Extrapolated CO2 profiles observed on August 7, 9, and 10, 2018, over Jiansanjiang. Red, blue, and yellow solid lines show the aircraft-based (in situ) data collected on August 7, 9, and 10, respectively, averaged for each flat stage of the flight. Dotted lines show the extrapolated parts of the profiles, with colors corresponding to sampling dates in accordance with the solid lines. Black horizontal lines show the tropopause height from NCEP reanalysis data.

Table 1. XCO2 derived from aircraft on each observation day (August 7, 9, and 10). OCO-2 (V9r) XCO2 were from August 5, which was the closest time point of XCO2 data from OCO-2 over Jiansanjiang to the observation period. Differences between aircraft XCO2 and OCO-2 are shown in the fourth (ppm) and fifth (%) columns. The average difference and standard deviation are shown in the fifth row.

Date	Aircraft* (ppm)	OCO-2 (ppm)	Difference (ppm)	$\frac{\text{OCO-2-Aircraft}}{\text{Aircraft}}\cdot 100\%$ (%)
August 7, 2018	398.33		−1.42	−0.35
August 9, 2018	401.62	396.91	−4.71	−1.17
August 10, 2018	397.95		−1.04	−0.26
		Average (1σ)	−2.39 (2.02)	−0.59 (0.44)

*The effect of the average kernel was taken into consideration for OCO-2.

Table 2. Aircraft integration error budget. Errors in the three profiles from multiple error sources contributed to the calculation results of the integrated total column. The error is spilt into four sources, similar to previously described error budgets (Wunch et

https://doi.org/10.5194/amt-2019-363
Preprint. Discussion started: 14 October 2019

Atmospheric Measurement Techniques Discussions

355 **al., 2017): the contribution from the aircraft profile itself, the contribution from the unknown surface to the bottom of the profile, the contribution from the upper troposphere and stratosphere, and error from the tropopause height.**

Date	Aircraft error (ppm)	PBL error (ppm)	Upper troposphere and stratosphere error (ppm)	Tropopause height error (ppm)
August 7, 2018	0.07	0.06	0.29	0.66
August 9, 2018	0.07	0.06	0.34	0.03
August 10, 2018	0.06	0.07	0.28	0.01
Average (1σ)	0.07	0.06	0.30	0.23